Thermal evolution and resources of the Bowland Basin (NW England) from apatite fission-track analyses and multidimensional basin modelling

Bhavik Harish Lodhia[1,2]*, Adeline Parent[3], Alastair J. Fraser[1], Martin Nuemaier[1] and Jan A. I. Hennissen[4]

[1]Department of Earth Science and Engineering, Imperial College London, South Kensington Campus, London SW7 2AZ, UK

[2]University of New South Wales, Kensington, Sydney 2052, Australia

[3]Schlumberger Plc., Ritterstr. 23, Aachen, North Rhine-Westphalia, Germany

[4]British Geological Survey, Keyworth, Nottinghamshire, NG12 5GG, UK

BHL, 0000-0002-3764-2248

*Correspondence: b.lodhia@unsw.edu.au

Abstract: Once highlighted for having significant shale gas resource potential, the Bowland Basin has been at the centre of both scientific and political controversy over the last decade. Previous shale gas resource estimates range from 10^3 to 10^1 TCF. Repeated events of induced seismicity following hydraulic fracturing operations led to an indefinite government moratorium and abandonment of operations across the mainland UK. We use apatite fission-track analyses to investigate the magnitude and timing of post-Triassic uplift and exhumation. Results indicate that maximum palaeotemperatures of 90–100°C were reached in the stratigraphically younger Sherwood Sandstone. We combine palaeotemperature predictions to constrain palaeo heat flow and erosion in regional basin models for the first time. Our results indicate variable maximum Late Cretaceous palaeo heat flow values of 62.5–80 mW m^{-2} and the removal of 800–1500 m of post-Triassic strata at wells across the basin. Regional 2D basin modelling indicates a gas-in-place estimate of 131 $\pm$ 64 TCF for the Bowland Shale. This reduces to a resource potential of 13.1 $\pm$ 6.4 TCF, assuming a recovery factor of 10%. These values are significantly lower than previous resource estimates and reflect the highly complex nature of the Bowland Basin and relatively unknown history of post-Triassic uplift, exhumation and erosion.

This chapter explores the thermal, uplift and erosional history of the Bowland Basin (NW England) using apatite fission-track analysis (AFTA). We apply these results to define new thermal and erosional histories across the Bowland Basin and estimate shale gas resource potential from 1D and 2D basin and petroleum systems modelling.

Geological setting and importance

The Bowland Basin trends NE–SW and lies between the Askrigg–Bowland High to the north and the Central Pennine High to the SE at an elevation of <500 m above mean sea level (Fig. 1, Gawthorpe 1986). It is one of several Early Carboniferous extensional basins that extend through Ireland to the Canadian Maritimes, formed by north–south extension associated with the opening of Paleothethys (Dewey 1982; Guion *et al.* 2000; Torsvik *et al.* 2002; Fraser and Gawthorpe 2003). Fault reactivation, extension and volcanic activity associated with the subduction and closure of the Paleothethys Ocean resulted in basin formation north of the Carboniferous Variscan Front across central Britain (Timmerman 2004). Structural, sedimentological, gravity and magnetic data suggest that although the present-day structural configuration is mainly a result of compression/transpression during late Carboniferous times, Dinantian tectonics and sedimentation were dominated by normal and transfer fault systems related to regional extensional transtension (Gawthorpe 1987). The Bowland Basin was exhumed during the Variscan Orogeny, and structurally inverted and folded into NE–SW-trending Caledonian en echelon folds (Arthurton 1983, 1984; Corfield *et al.* 1996). Very thick accumulations of Dinantian rocks, comprising carbonates and terrigenous mudstones with rare sandstones (>2 km), have been reported in the literature (e.g. Earp *et al.* 1961; Charsley 1984; Gawthorpe 1986; Andrews 2013; Clarke *et al.* 2018). However, within the basin no pre-Carboniferous rocks are known and the base of the Dinantian sequence is not proven. The youngest rocks in the basin are of Triassic age (Fig. 2), with over 200 Ma of missing stratigraphy.

From: Emmings, J. F., Parnell, J., Stephenson, M. H. and Lodhia, B. H. (eds) 2024. *The Bowland Shale Formation, UK: Processes and Resources*. Geological Society, London, Special Publications, **534**, 39–60.
First published online January 13, 2023, https://doi.org/10.1144/SP534-2022-15

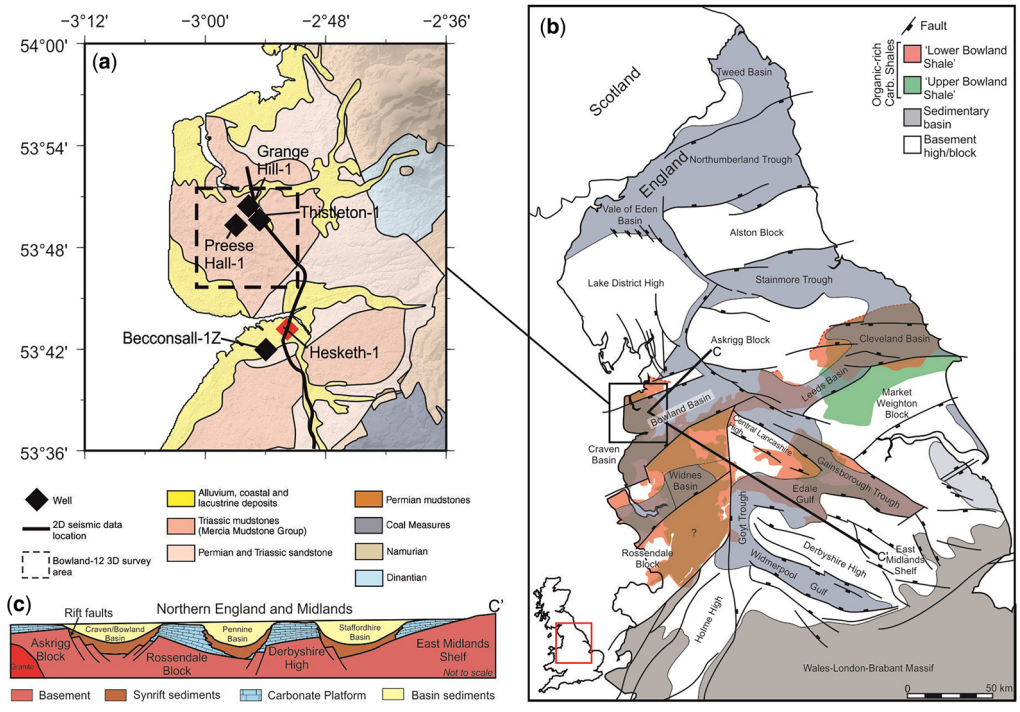

Fig. 1. Geological map, study area with data locations and representative cross section. (**a**) Geological map of Bowland Basin with locations of wells and seismic data used in this study. The red diamond marks the location of Hesketh-1, used for apatite fission track analysis. The location of the region is indicated by the black rectangle in (b). (**b**) Major faults, sedimentary basins and coverage of Bowland Shale formation across northern and central England. Distribution of Bowland Shale from Andrews (2013) and positions of faults from Fraser and Gawthorpe (1990). (**c**) Schematic profile across the Central Province showing the general style of 'blocks' and 'basins' that are typical for northern England and the Midlands at the end of the Dinantian. This figure is not accurately scaled, either vertically or horizontally. The maximum depth of basinal areas is *c.* 500–800 m and the profile location is given for indicative purposes only. Source: (a) adapted from Donnelly (2006) and (c) adapted from Collinson (1988).

Source rocks of the Bowland Basin

The main hydrocarbon source rocks in the basin are the regional Bowland Shale group, which is composed of the Pendleian–Arnsbergian Carboniferous post-rift Upper Bowland Shale, Asbian–Brigantian synrift Lower Bowland Shale and the Early Carboniferous Bowland–Hodder Formation (Figs 1 & 2). With a combined thickness of over 1000 m in the Bowland Basin, the Bowland–Hodder sequence of shales is one of the thickest known potential self-sourced, unconventional hydrocarbon resources in the world. The strata are organic rich with total organic carbon (TOC) values of between 1 and 7%, with an average of 2.65%, and organic maturity that ranges from the upper oil window in the higher part of the section to dry gas (Ro = 2.4%) in the Lower Bowland Shale (Clarke *et al.* 2018). The palaeogeography of northern and central England and the deposition of the Bowland Shale were primarily controlled by the progression of the Variscan collision-type orogeny, whereby the Variscan plate cycle controlled the development of synrift, post-rift and inversion megasequences from Late Devonian to early Permian times. Sequences developed within these Carboniferous megasequences are primarily controlled by episodic rifting and periodic fault reactivation with eustatic sea-level changes providing only minor control at the subsequence level, mainly observed during the post-rift phase (Fraser and Gawthorpe 1990). Different palaeogeographic environments existed between basement blocks across northern and central England during the Carboniferous. For example, during the Late Holkerian–Mid Asbian, the Bowland Basin was flanked to the north and south by regional carbonate highs and dominated by marine-influenced turbidite conditions sourced from the west. The Cleveland Basin in NE England was dominated by open marine conditions, with rimmed shelf

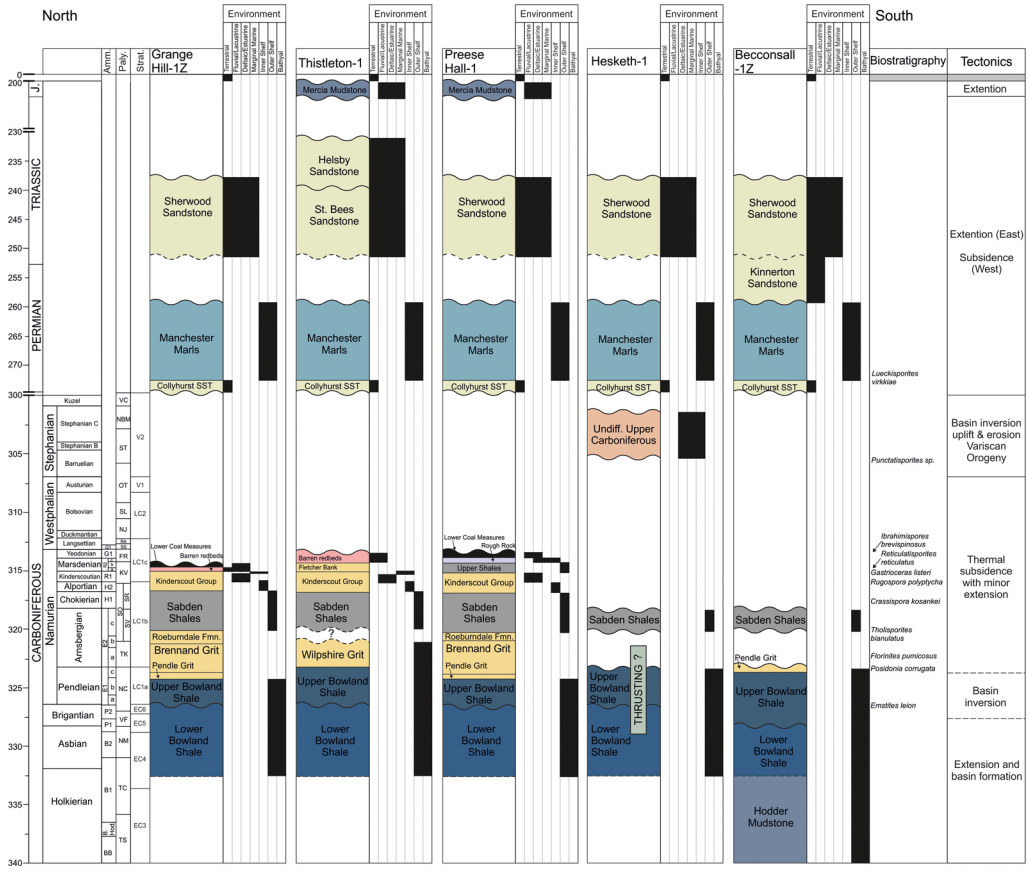

Fig. 2. Biostratigraphy, PWDs and tectonic histories of wells used in this study. Biostratigraphy data are sourced from well completion reports. Stratigraphy and tectonic history after Fraser and Gawthorpe (1990). Environments correspond to PWDs defined by Immenhauser (2009).

conditions dominating the Staffordshire Basin and West Midlands. By Late Asbian–Early Brigantian times, deepwater facies sourced from the west dominated the Bowland Basin, whereas the Cleveland Basin was dominated by carbonate ramp facies and the West Midlands was dominated by a drowned carbonate shelf environment (Fraser and Gawthorpe 2003). Hence, it is important to recognize that age-equivalent Carboniferous shales deposited across northern and central England are highly heterogenous and sourced from different palaeogeographic regions.

Across northern and central England, the Bowland Shale possesses all the source rock properties necessary to produce unconventional shale gas. The Bowland Shale holds a significant shale gas/liquid potential in areas with appropriate geochemical properties. This includes a TOC content of 1–7%, gas-prone organic matter (type II/II kerogen), thicknesses up to 620 m and thermal maturity values in the thermogenic gas window across large areas of northern and central England (Collinson 1988; Fraser and Gawthorpe 1990; Gross *et al.* 2015, Fig. 1). However, a substantial portion of the literature (e.g. Andrews 2013) confusingly applies the same age to the different sub-units of the Bowland Shale and assumes the interval to be homogenous across northern England and the Midlands. In reality, the highly compartmentalized nature of northern and central England's sedimentary basins and the differing sources of source rock material feeding into these basins mean that Carboniferous shales across this region of the same age in different basins have variable properties. From Clarke *et al.* (2018), an approximate value of 3583 square miles (or 9281 km^2) is used for basin area. The tectono- and biostratigraphic history of five wells from across the Bowland Basin assessed in this study is summarized in Figure 2.

Recent exploration and cessation of hydraulic fracturing operations

The Bowland Basin has long been a region of economic interest, with Triassic reservoirs sourced from Carboniferous shales comprising the main play type. Examples include the onshore Formby Oil Field (Falcon and Kent 1960) and offshore Manx–Furness Basin (Pharaoh *et al.* 2018). From 1960 to 2000, a number of conventional exploration wells were drilled in the Bowland Basin, including the important Thistleton-1, Hesketh-1, Elswick-1, Swinden-1 and Whitmoor-1 wells (Clarke *et al.* 2018). The only significant hydrocarbon discovery before 2000 was made at Elswick-1 in the Permian Collyhurst Sandstone, which produced following hydraulic fracturing in 1990. The reservoir trap is a four-way dip closure with cumulative production to date being 0.5 BCF (billion cubic ft).

Since 2011, several exploration wells have been drilled in the Bowland Basin to target the Bowland Shale for shale gas potential. Preese Hall-1 (2011), Grange Hill-1Z (2012), Preston New Road-1 (PNR-1, 2014) and Preston New Road-2 (PNR-2, 2018) were drilled by Cuadrilla Resources and penetrated the Lower Bowland Shale. The region is highly structured and a significant number of near-vertical faults make seismic interpretation very difficult (e.g. Anderson and Underhill 2020). The primary cause of induced seismicity in the region is believed to be the reactivation of faults (Nantanoi *et al.* 2022). Repeated incidents of induced seismicity above the UK's upper limit of $M_w = 5$ caused operations to be ceased whilst the causes were investigated. In November 2019, the UK Government announced an indefinite moratorium on all hydraulic fracturing activities following an incident of induced seismicity ($M_w = 2.9$) at the Preston New Road site, Lancashire. This major shift in government policy effectively marked the end for onshore UK shale gas operations at the time of writing.

History of resource estimates

Resource estimates for the Bowland Shale vary wildly. Andrews (2013) estimated gas in place (GIP) for the Bowland–Hodder unit across the entire northern and central England to be between 164 and 477 TCF (trillion cubic feet). Andrews (2013)'s assessment was based on adsorbed and free gas estimates for US shales, and assumed that all Bowland Shale source rock with a maturity above 1.1% Ro had already generated gas. Cuadrilla Resources estimated the gas per unit volume of rock in the Bowland Shale to range from 0.6 to 1.5 BCF per metre per square mile (Clarke *et al.* 2018). Their assessment indicated oil generation in the Late Carboniferous, before Variscan uplift, with renewed subsidence through the early Mesozoic resulting in increased maturity and gas generation. Note that this resource estimate refers specifically to the Bowland Basin and not the total area of coverage of the Bowland Shale across northern and central England (e.g. Andrews 2013). Owing to an abundance of well testing data from US shale gas wells, recovery factors are often based on US analogue data and typically vary from 20 to 30% (US Energy Administration Information 2015). However, reliable recovery factor estimates are dependent on data from extensive well production testing across geological formations, which at the time of writing are not available in the UK. Given the significantly increased geological complexity of northern England sedimentary basins and geochemical variability of the Bowland Shale, we do not apply recovery factors based on US analogues in our resource estimates. Recent studies estimated a recovery factor as low as 10% for the Bowland Shale (e.g. Whitelaw *et al.* 2019).

Whitelaw *et al.* (2019) use sequential high-pressure water pyrolysis to replicate petroleum generation and expulsion in uplifted onshore basins and predict the maximum GIP using oil window and gas window mature UK Bowland Shales. Their method gives an estimated maximum total GIP of 140 $\pm$ 55 TCF. Assuming a lower economic recovery factor of 10%, which is likely for much of the Lower Bowland Shale owing to its depth of over 3000 m, Whitelaw *et al.* (2019)'s estimate represents a maximum resource estimate of 14 $\pm$ 6 TCF, less than 10 times the previous estimate.

Although the future of shale gas exploration in the Bowland Basin looks uncertain, the region presents several important scientific challenges. First, the history of uplift, erosion and palaeo heat flow of the region is poorly constrained. These are important parameters that affect the burial and maturation of source rocks, and ultimately the generation and timing of migration of hydrocarbons. Previous attempts to estimate resources have been focused on laboratory analyses and comparisons to analogue data from US shales. However, regional basin and petroleum systems modelling that combines geology at the borehole scale with geophysics at the basin scale has never before been attempted in the region. Furthermore, there have been no attempts to date to reconcile uncertainties in regional post-Jurassic uplift/erosion using AFTA as an aid for basin modelling in the Bowland Basin. Understanding these processes may shed light on the possibilities beyond unconventional shale gas. This includes potentially using of the Bowland Shale to produce low-carbon resources via CO_2 sequestration or investigating its potential as a geothermal reservoir in the naturally fractured Triassic Sandstone (e.g. Sherwood Sandstone).

Missing stratigraphy and palaeotemperature

There have been two major phases of uplift and erosion across the Bowland Basin since its formation. Basin inversion in the foreland of the Variscan orogenic belt occurred in the late Westphalian and was related to events to the south. The climax of inversion occurred in the late Westphalian D–Stephanian and resulted in extensive uplift and erosion of the Variscan foreland. As a consequence, post-Carboniferous rocks of various ages rest upon Carboniferous rocks with angular unconformity over most of the British Isles, which is evident in seismic data throughout the province (Corfield *et al.* 1996). Estimates of burial and uplift obtained from seismic, vitrinite reflectance (VR) and fission-track data indicate the removal of 2000–2500 m of Late Carboniferous stratigraphy owing to Variscan erosion (Fraser and Gawthorpe 1990). This is evident from the absence of Westphalian/Stephanian strata in wells across the basin (Fig. 2). This event is marked by a regional unconformity that separates underlying Carboniferous strata from Permian clastic sediments and is named the Base Permian Unconformity (Fig. 3).

The second phase of uplift and erosion across the region is responsible for the absence of post-Triassic stratigraphy across the majority of the Bowland Basin and continues to the present day. There is around 200 Ma of missing stratigraphy in the Bowland Basin (Fig. 2). The evolution of the region from fluvial/lacustrine–marginal marine conditions to its present terrestrial setting is therefore not recorded.

Early application of AFTA to exploration wells from the East Irish Sea Basin (EISB) revealed early Neogene palaeotemperatures of around 110°C or more. Further studies in the Irish Sea and adjacent areas, using a combination of AFTA and VR, indicated at least three additional palaeothermal episodes (periods of elevated heating or cooling): pre-Permian (>290 Ma), Late Permian to mid-Triassic (260–220 Ma) and Early Cretaceous (140–110 Ma). Other evidence of early palaeothermal effects, for which timing is only constrained to the interval 300–150 Ma, may reflect these or additional episodes (Green *et al.* 1997). The Bowland Basin lies on the eastern margin of the larger Permian–Mesozoic EISB, with peak hydrocarbon generation from the Bowland source rocks coincident with maximum burial of the system during Late Jurassic–Early Cretaceous times (Pharaoh *et al.* 2018). The AFTA conducted by Holford *et al.* (2005) revealed several distinct episodes of kilometre-scale exhumation during Early Cretaceous (<3 km), Early Paleogene (<2 km) and late Paleogene–Neogene times (*c.* 1 km), with the overall magnitude of exhumation in each episode decreasing through time. Regional Early Cretaceous exhumation appears to be related to incipient Atlantic rifting. Early Paleogene exhumation was driven by a combination of localized tectonic inversion and regional epeirogenic uplift, although early Paleogene palaeotemperatures within parts of the Irish Sea basin system are dominated by non-burial-related processes. A final phase of exhumation related to late Paleogene– Neogene tectonic inversion uniformly removed *c.* 1 km of section from this region (Holford *et al.* 2005). Furthermore, mapping of exhumation patterns in the EISB through sonic velocity analyses of overcompacted Upper Triassic shales by Holford *et al.* (2009) indicated that the sub-Quaternary unconformity present across the EISB marks between 1.3 and 3.3 km of post-Early Jurassic exhumation.

It is highly probable that the Bowland Basin was also affected by the exhumation and erosion of the EISB. However, there are no studies that combine palaeotemperature measurements with regional basin modelling in the Bowland Basin. In this study, we use apatite fission-track data from well Hesketh-1 (Fig. 1) for the first time to measure palaeotemperatures in the Bowland Basin over the interval of missing stratigraphy and apply this constraint to 1D and regional 2D basin and petroleum systems modelling.

Basin modelling relies on fitting evolution curves to maturity data, whereby different combinations of uplift/erosion and palaeo heat flow can yield results that adequately fit the data. As such, in the absence of other geological information, it is not possible to determine a unique solution to fit maturity data alone. This presents a significant challenge in the Bowland Basin owing to the amount of missing stratigraphy. In this study, we apply AFTA to estimate palaeotemperatures of the Triassic Sherwood Sandstone at Hesketh-1 and use this to constrain estimates of post-Triassic erosion at wells across the Bowland basin using 1D basin modelling. Estimates of post-Triassic erosion are used to constrain 2D basin modelling for the first time and to estimate the shale gas resource potential of the Bowland Basin.

Whilst VR data may be applied to determine maximum thermal maturity, the application of AFTA allows the most likely temperature–time histories of samples to be determined. In this study, we use AFTA to determine the timing and magnitude of maximum palaeotemperatures and apply these to calibrate 1D and 2D basin models obtained from five wells and a regional seismic profile across the Bowland Basin, respectively. Finally, we extrapolate our results across the basin area to estimate the magnitude of in-place shale gas resources in the Bowland Basin.

Thermal history from apatite fission-track data and application to 1D basin modelling

As temperature increases progressively with depth within the lithosphere, palaeothermal indicators

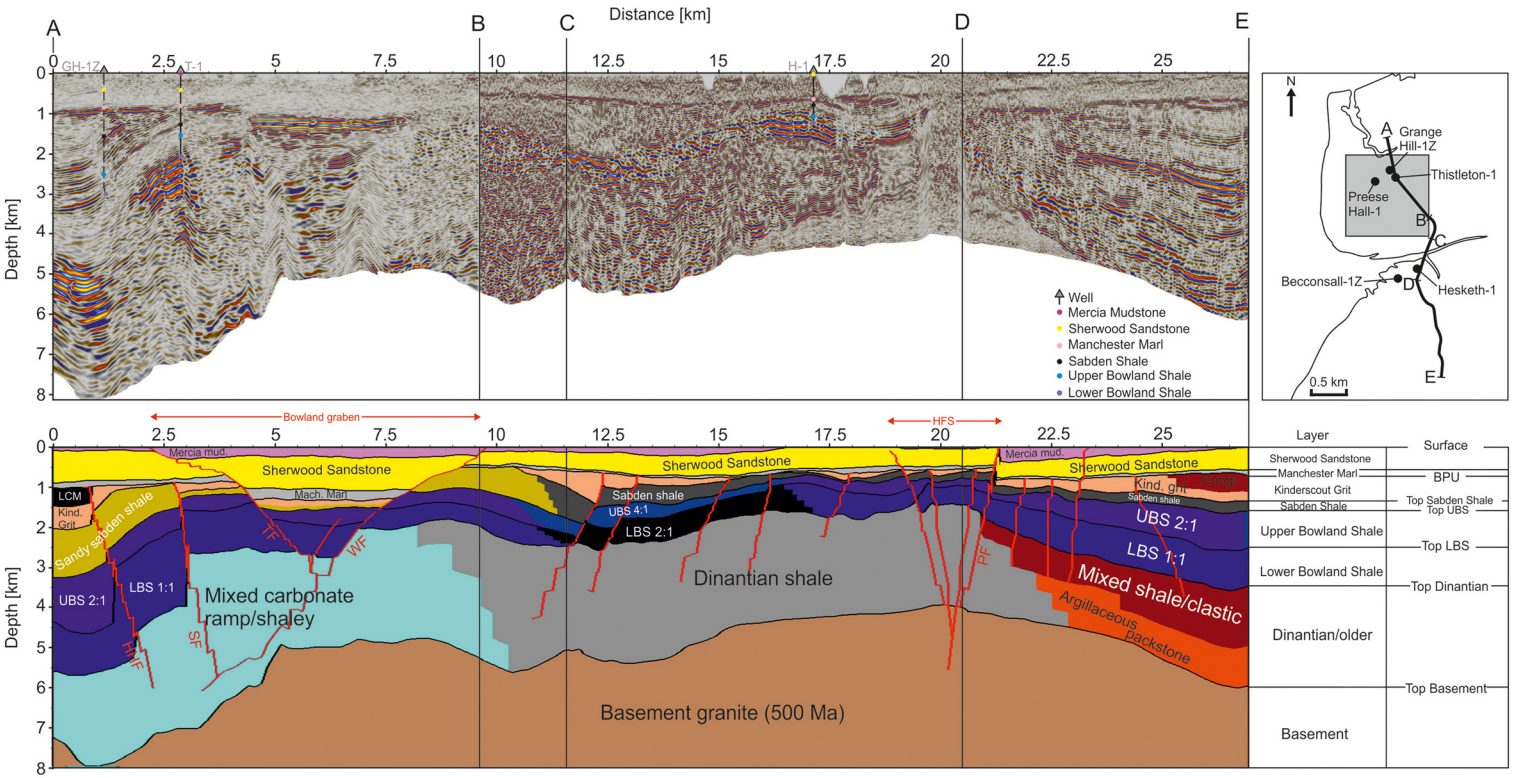

Fig. 3. Depth converted sesicmic data and facies model used in basin modelling. Depth conversion performed using checkshot data from wells and the UK Onshore Geophysical Library. Faults and structures are labelled in red: HFS, Hesketh flower structure; HHF, Heaves Ho Fault; PF, Pendle Fault; SF, Summerer Fault; TF, Thistleton Fault; WF, Woodsford Fault. LBS, Lower Bowland Shale; LCM, Lower Coal Measures; UBS, Upper Bowland Shale. Shale–clastic ratios determined from Carboniferous palaeogeographies are applied to the UBS and LBS (e.g. Fig. 7).

such as AFTA and VR can be used to access the former burial depths of rock units (Green *et al.* 2002). Sedimentary units are progressively heated during burial and begin to cool at the initiation of exhumation. AFTA and VR data provide quantitative estimates of the temperatures attained by individual rock samples at a palaeothermal maximum, prior to the onset of cooling (Green *et al.* 1995, 2002). Vitrinite reflectance data can provide discrete estimates of maximum post-depositional palaeotemperatures, whilst AFTA can provide either upper or lower limits or a range of values for the maximum palaeotemperature in up to three separate palaeothermal episodes (Bray *et al.* 1992; Green *et al.* 2002).

In exhumed basins like those of the Irish Sea, palaeotemperatures derived from AFTA and VR data through a vertical rock section can be used to estimate palaeogeothermal gradients (e.g. Holford *et al.* 2005, 2009). Moreover, by extrapolation to an assumed palaeosurface temperature, the thickness of sections removed during exhumation can be quantified (Green *et al.* 2002; Holford *et al.* 2005). Full methodological descriptions of the analytical and interpretative procedures by which thermal history data are extracted from apatite and vitrinite samples are provided by Green *et al.* (2001, 2002).

Temperature history reconstruction using QTQt for Hesketh-1

Many recent attempts to model time–temperature histories of rocks from thermochronologic data have taken advantage of one of two freely available software packages: HeFTy (Ketcham *et al.* 2015) and QTQt (Gallagher 2012).

Employing a Bayesian transdimensional Markov chain Monte Carlo (MCMC) inversion scheme, QTQt constrains a set of best-fit temperature–time paths given a posterior probability distribution (Gallagher 2012). Essential input parameters for models using this program are: the number of fission tracks per unit volume (N_s), the number of induced tracks per unit volume (N_i), the composition (given as wt% Cl), track lengths (in μm), the *C*-axis angle, the calibration factor used in the external detector method (ζ), the number of tracks counted in the dosimeter (N_d), the induced track density (ρ_D), the present-day temperature (T_p), the depth (Z) and the geographic coordinates (X and Y from the British National Grid coordinates). Primary QTQt model outputs include three time–temperature models:

- The maximum likelihood (ML) model is the model that fits the measured data the best but is the most complex.
- The maximum posterior (MP) model is the simplest model, where the posterior probability is proportional to the likelihood multiplied by the prior (no uncertainties are associated with the MP or the ML models).
- The expected (EX) model is essentially a weighted-mean model of intermediate complexity between the ML and MP models, where the weighting is provided by the posterior probability of each model solution. The iterative MCMC sampling can be used to calculate the uncertainty for the EX model and define the 95% credible interval (Bayesian equivalent to the confidence interval) around the EX-model solution.

The QTQt software allows resampling of thermochronometric ages, commonly by assuming a normal distribution (the standard deviation) centred on the measured radiometric age (N_s/N_i ratio) or, alternatively, resampling of the chosen kinetic parameter (i.e. measured Cl value), which is a way of recognizing uncertainty in laboratory-calibrated kinetic models extrapolated to geological timescales (McDannell *et al.* 2022).

Apatite fission-track data were obtained from two samples, GC402-17 and GC402-18, within the Triassic Sherwood Sandstone at Hesketh-1 (Fig. 1) at depths of 145 and 521 m, respectively. The original data were obtained by Geotrack Intl and recently reprocessed to include compositional and *C*-axis angle information (Tables A1–A4 in the Appendix).

Bayesian transdimensional MCMC inversion modelling results obtained using QTQt (Gallagher 2012) for Hesketh-1 are shown in Figure 4. The results for the deeper sample, GC402-18, indicate a greater degree of cooling between 80 and 50 Ma with a maximum Late Cretaceous palaeotemperature of 90–100°C. The results for the shallower sample, GC402-17, indicate maximum Late Cretaceous palaeotemperatures of 80°C. The EX, ML and MP models for both samples show cooling from maximum Late Cretaceous palaeotemperatures of 90–100°C over 110–75 Ma to the present.

Application to 1D basin modelling

Basin modelling is defined as the numerical simulation of basin development and processes through geological time (Hantschel and Kauerauf 2009). The results demonstrate the burial history of sediments and combine geological information that includes formation thickness, age, porosity and lithotype to predict the evolution of geological horizons. Petroleum systems modelling combines basin models with source rock properties and palaeothermal history to determine the potential generation of hydrocarbons, fluid migration and the likelihood of retention through structural or stratigraphic trapping. In our study, all basin modelling results were calculated using Schlumberger PetroMod© software.

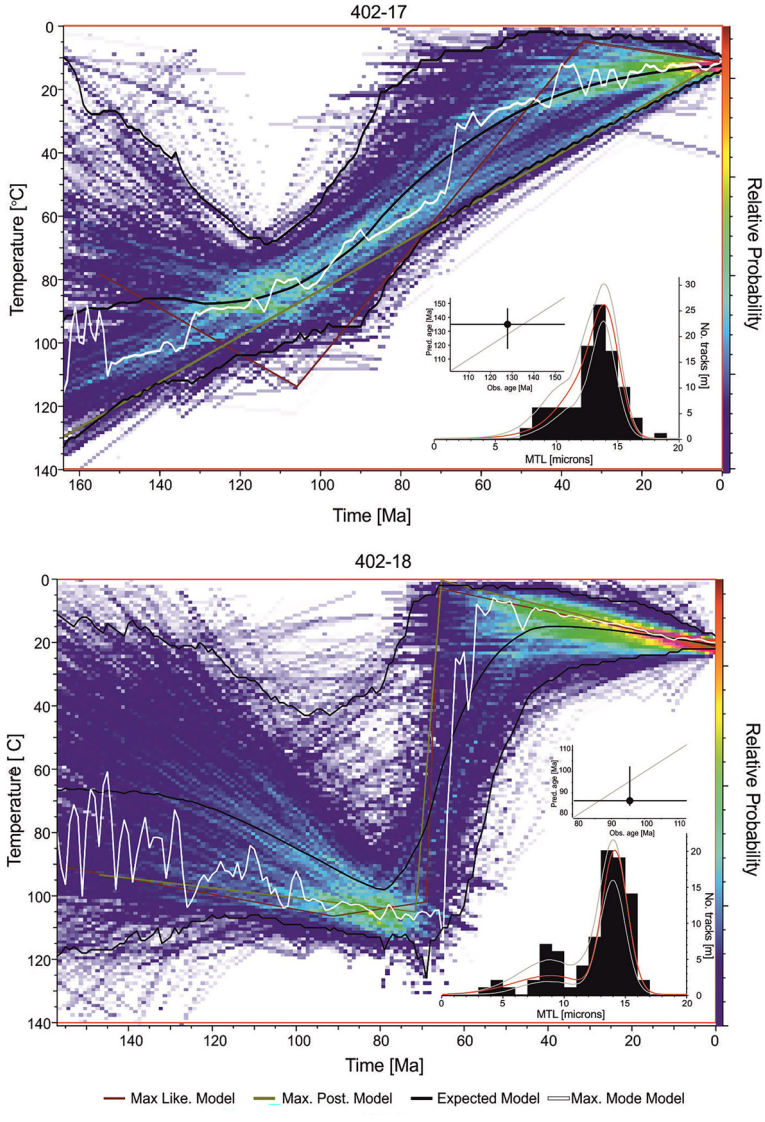

Fig. 4. The AFTA modelling results for samples GC402-17 and GC402-18 from Hesketh-1. MTL, mean track length (μm).

The input parameters and thermal boundary conditions used in the assessment of wells in the Bowland Basin included:

- The palaeowater depth (PWD, in m) was determined by examining palaeomaps, specific facies, biostratigraphy and time of deposition, which allowed the approximation of sea levels in the study area (see Fig. 2 for PWDs in each well). In accordance with the definition of depositional environments as described by Immenhauser (2009), the PWDs of the wells evaluated in this study ranged between terrestrial (present day) and bathyal (>2000 m).
- The synthesized sediment–water interface temperature (SWIT, in °C), which normally varies over time, was calculated using an in-built function Wygrala (1989). The model calculates appropriate temperatures over time after applying the study area's specific latitude and region. The SWIT ranged from 5 to 25°C in the studied area.

- the palaeo heat flow (in mW m^{-2}). A present-day heat flow value of 55 mW m^{-2} is also used (Downing and Gray 1986) for the region.

Owing to a lack of geological data owing to uplift and erosion over the last 200 Ma and based on the AFTA results from Hesketh-1 in this study, a constraint of Late Cretaceous palaeotemperatures of 90–100°C within the Sherwood Sandstone is applied to the wells Grange Hill-1Z, Preese Hall-1 and Thistleton-1 (Fig. 5). Post-Jurassic deposition, erosion and Late Cretaceous–present heat flow values were varied to produce maturity profiles that correspond with measured VR data (where available).

Regional stratigraphic (thickness) and VR (palaeoburial) studies were used to estimate the degree of uplift and subsequent erosion of synrift and post-rift Carboniferous sediments in NW England. These studies highlight the extent to which basins such as Bowland and Northumberland, which are interpreted as lying normal to the NW–SE direction of maximum compressive stress, were inverted during the Variscan (Fraser and Gawthorpe 1990). Estimates of Variscan erosion in the Bowland Basin range between 2000 m in the north and *c.* 2500 m in the south. Hence, a value of 2300 m is used for Hesketh-1 and 2000 m is used for Grange Hill-1Z, Preese Hall-1 and Thistleton-1 in the north of the basin. It is also important to note the absence of Namurian (Arnsbergian and Chokierian–Yoredonian) stratigraphy at Hesketh-1 (Fig. 2). Based on the thickness of Namurian intervals encountered at other wells in the region, a value of 200 m was chosen for Namurian erosion at Hesketh-1.

1D basin modelling results for Hesketh-1 calculated using maximum Late Cretaceous heat flow values = 70–90 mW m^{-2} and erosion = 800–1500 m all match the maturity data (Fig. 6). However, only heat flows of 70–80 mW m^{-2} and erosion of 1200–1500 m allow the Sherwood Sandstone to reach a palaeotemperature of 90–100°C, with higher heat flow corresponding to lower erosion values. Furthermore, the large offset in the VR profile at the Variscan unconformity produced for heat flow = 90mW m^{-2} and erosion = 800 m at Hesketh-1 (red line in Fig. 6a) is inconsistent with the small/miniscule offsets seen at all other wells analysed in this study.

The results for Grange Hill-1Z indicate maximum Late Cretaceous heat flow = 62 mW m^{-2} and erosion = 1450 m, as higher heat flow/lower erosion scenarios either do not match calibration data or do not produce adequate palaeotemperature in the Sherwood Sandstone. The results for Preese-Hall-1 indicate maximum Late Cretaceous heat flow = 80–90 mW m^{-2} and erosion = 700–850 m. The results for Thistleton-1 indicate maximum Late Cretaceous heat flow = 62.5–65 mW m^{-2} and erosion = 1000–1200 m.

Resource potential from regional 2D basin modelling

The results from 1D basin modelling (Figs 5 & 6) indicate maximum Late Cretaceous heat flow and erosion of 62.5–65 mW m^{-2} and 1000–1450 m, respectively, at Grange Hill-1Z and Thistleton-1 in the north of the Bowland Basin and values of 70–80 mW m^{-2} and 1200–1500 m at Hesketh-1 in the south. Figure 3 shows a north–south-oriented regional composite seismic line that crosses the majority of the Bowland Basin, produced using the 100 km^2 Bowland-12 3D seismic survey and data provided by Beneath Britain, University of Oxford, UK. This line intersects Thistleton-1 in the north and Hesketh-1 in the south. The position of Grange-Hill-1Z is projected onto Figure 3; however, the well is located <1 km away from the seismic profile. Data from the Bowland-12 3D seismic survey (shot by Cuadrilla 2012) and 2D seismic lines GC82–343 (shot by Horizon 1982), GCE-86-360 (shot by Horizon 1986) and UKOGL-RG-006 are combined to generate a regional composite line that intersects Thistleton-1 and Hesketh-1 and extends north–south across the Bowland Basin (Fig. 3). Checkshot data for Thistleton-1 and Hesketh-1 from the UK Onshore Geophysical Library (UKOGL) was used to constrain seismic velocities and depth convert seismic data.

Sedimentary facies assignment

The facies maps used to build the 2D model were generated by combining the existing regional facies interpretation (Fraser and Gawthorpe 1990), borehole data and seismic stratigraphy. Within the Bowland Basin, the Bowland Shale is interpreted to have been sourced by rivers delivering sediments from basement highs in the north. This contrasts with deposition of the Bowland Shale in sub-basins to the east, e.g. the eastern part of the Gainsborough Trough was influenced by distal clastic input sourced from the Fenno-Scandian landmass to the NE (Palci *et al.* 2020). Palaeogeographic reconstructions from Fraser and Gawthorpe (1990) were used to infer the position of the shelf edge, basin centre and regions of increased clastic/carbonate influence during Early Carboniferous rifting (Fig. 7). The proportion of clastic to non-clastic sediment is inferred to decrease towards the basin centre. Shale–clastic ratios for Lower and Upper Bowland Shales are inferred as 2:1 and 4:1 in the centre of the basin and 1:1 and 2:1 at the edges of the basin, respectively. The increased clastic influence in the northern Bowland

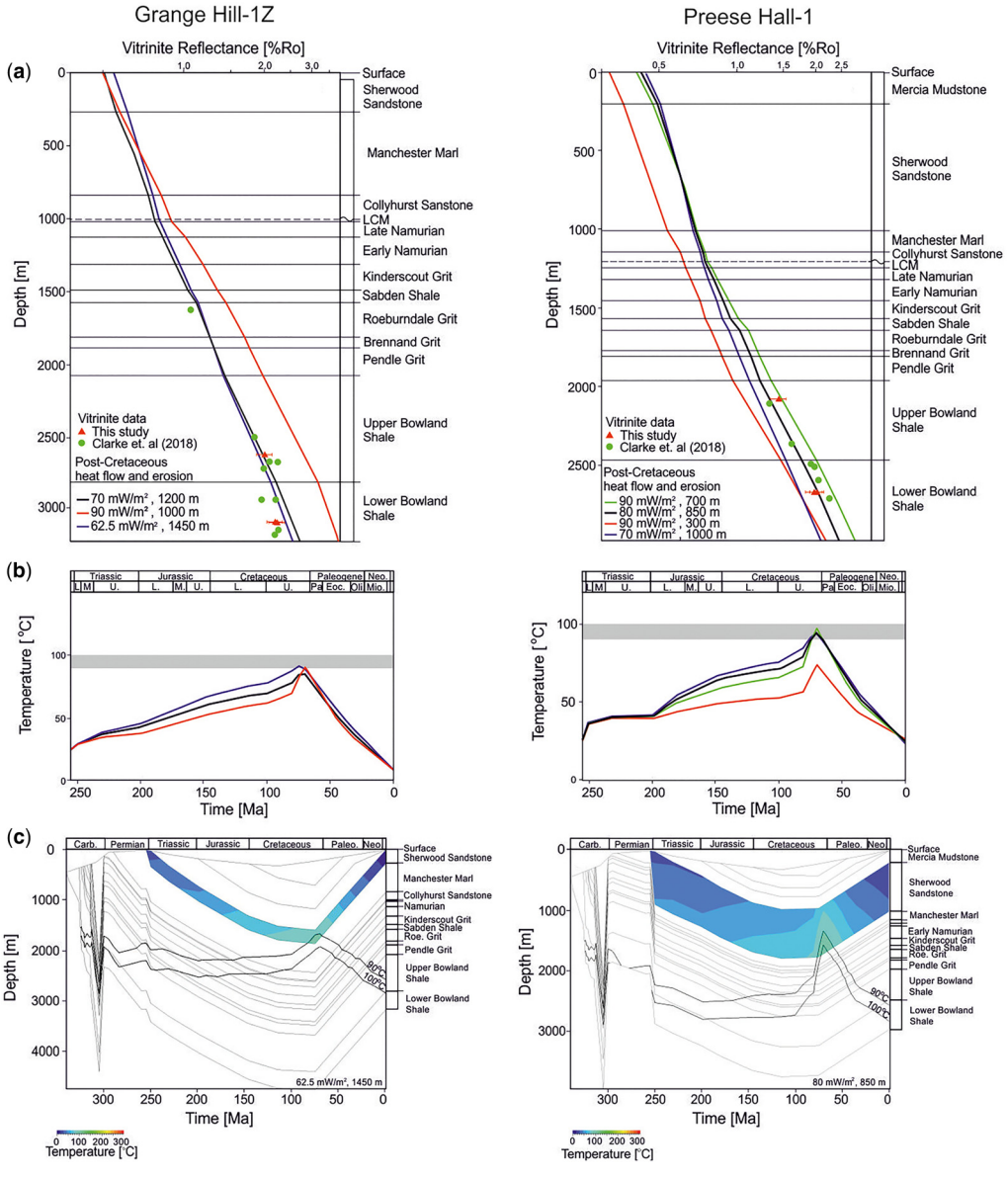

Fig. 5. 1D basin modelling results for Grange Hill-1Z, Preese Hall-1 and Thistleton-1. (**a**) Maturity plot calculated using Carboniferous erosion = 2000 m and post-Cretaceous erosion and heat-flow values as labelled. Arnsbergian stratigraphy missing in Hesketh-1 is present here. Dashed lines mark unconformities. (**b**) Temperature–time plot for Sherwood Sandstone. Results from AFTA (Fig. 4) indicate that end Cretaceous/Paleogene palaeotemperatures reached 90–100°C. (**c**) Burial history plot with palaeotemperature of Sherwood Sandstone. Black lines, 90–100°C isotherms. PWD values from biostratigraphy as shown in Figure 2. Maturity data used to calibrate models are from Clarke *et al.* (2018).

Basin is reflected by the inclusion of mixed sand/shale Sabden Shale sedimentary facies, and post-Carboniferous facies are assumed continuous across the basin.

Source rock properties and kinetics

Several important source rock properties must be considered to evaluate hydrocarbon generation

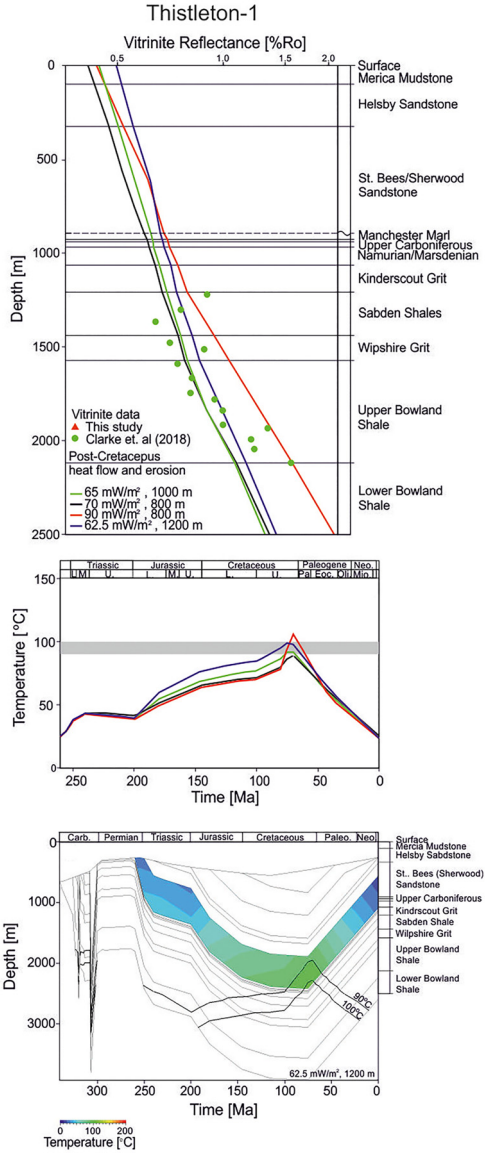

Fig. 5. *Continued.*

during basin modelling. These include the initial TOC (TOC_0), the initial hydrogen index (HI_0) and first-order kinetic parameters (i.e. the activation energies and frequency factors). Whilst the Bowland Shale is characterized by a vertical lithological variation that reflects both minor and major cycles of sea-level change and variations in carbonate and clastic input, analysis conducted on core in the Bowland Basin and Widmerpool Gulf suggests that the Bowland Shale yields a high and consistent TOC concentration (Gross *et al.* 2015; Clarke *et al.* 2018; Palci *et al.* 2020). Hence for simplicity, TOC_0 has been modelled as vertically homogeneous within the Bowland Shale (Palci *et al.* 2020).

The TOC_0 was estimated using a back-calculation involving measured present-day TOC, HI_0 and a modelled transformation ratio (TR) of the kerogen. Daly and Edman (1987), Peters *et al.* (2005) and Jarvie (2012) present different methods to back-calculate TOC_0, with the most widely applied method being:

$$TOC_0 = \frac{p\text{HI TOC}}{\text{HI}_0(1 - \text{TR})(p - \text{TR}) + \text{HI TOC}} \quad (1)$$

where $p = 83\%$ is the percentage of carbon in generated petroleum, the TOC is given as a percentage and the HI is in mgHC $gTOC^{-1}$, where HC is hydrocarbon (Peters *et al.* 2005). Transformation ratio values from a simulation with arbitrary HI_0 and TOC_0 values may be used to solve for TOC_0 by iteration. This is possible as the TR is not dependent on the initial HC mass (Hantschel and Kauerauf 2009).

The average TOC_0 values for the Upper and Lower Bowland Shale are: 2.71 and 1.3% at Thistleton-1 and 3.56 and 2.59% at Hesketh-1. The average HI_0 values for the Upper and Lower Bowland Shale are: 600 and 300 mgHC/gTOC at Thistleton-1 and 600 and 343 mgHC/gTOC at Hesketh-1. These values reflect the variation in type II and type II/III kerogen present in the Upper and Lower Bowland Shale. For 2D basin modelling, average TOC_0 values of 2.01 and 2.59% were applied for the Upper and Lower Bowland Shales, respectively. Average HI_0 values of 450 and 471 mgHC gTOC−1 were applied for the Upper and Lower Bowland Shales, respectively. The TOC values were varied by ± 50% to create low, medium and high modelling scenarios that reflect the variability of the Upper and Lower Bowland shale across the basin.

To predict the composition, masses and phases of hydrocarbons expelled from the Bowland Shale, a 14-component kinetic reaction (compositional phase kinetic) must be applied. The 14-component scheme is suitable for predicting phase properties such as the gas/oil ratio, American Petroleum Institute gravity and saturation pressure (Hantschel and Kauerauf 2009). Yang *et al.* (2015) analysed samples of Bowland Shale that contained immature marine type II kerogen. While this composition is generally typical for the Bowland Shale across northern England, the analyses of Yang *et al.* (2015) contained compositional differences between the whole rock and kerogen. Whole-rock samples are characterized by low HI and type III organic matter, whereas the kerogen shows high HI and type II organic matter. Hence, the kinetic reaction of Yang *et al.* (2015) may not be representative of the

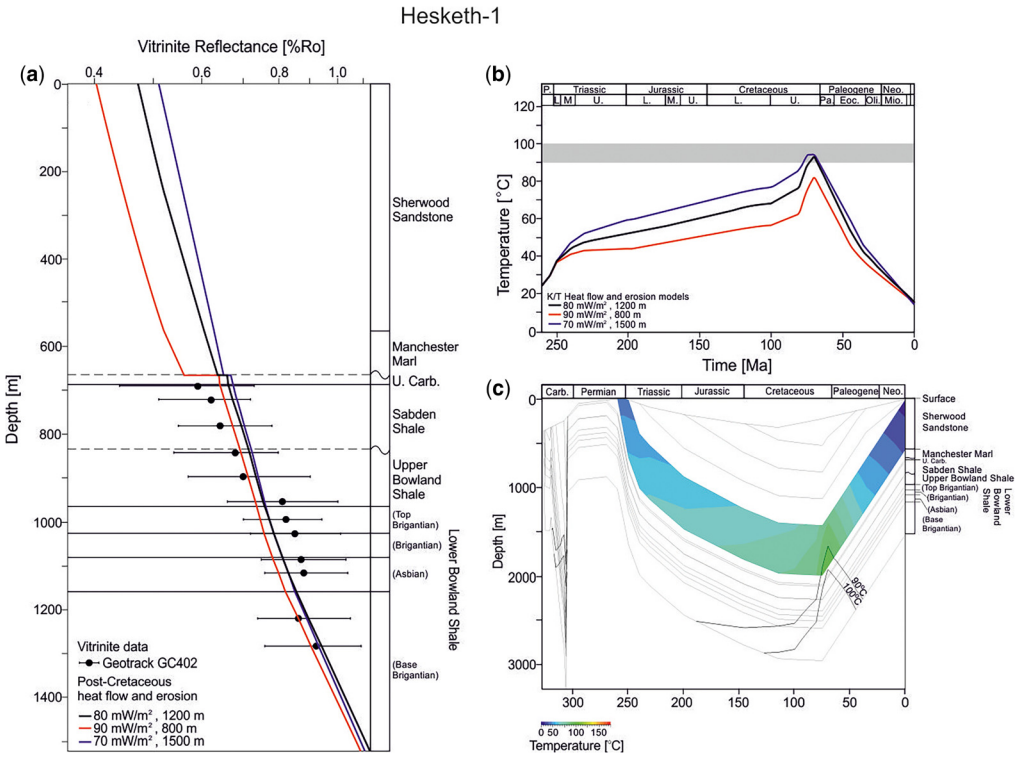

Fig. 6. 1D basin modelling results for Hesketh-1. Thrust faulting within the Carboniferous section (Lower Bowland Shale) is accounted for in this model. (**a**) Maturity plot calculated using Carboniferous erosion = 2000 m, Arnsbergian erosion = 100 m and post-Cretaceous erosion and heat-flow values as labelled. Dashed lines mark unconformities. (**b**) Temperature–time plot for Sherwood Sandstone. Results from AFTA (Fig. 4) indicate that end Cretaceous/Paleogene palaeotemperatures reached 90–100°C. (**c**) Burial history plot with palaeotemperature of Sherwood Sandstone. Black lines are 90–100°C isotherms. PWD values from biostratigraphy as shown in Figure 2. Maturity data used to calibrate model are from Green and Bray (1992).

Bowland Shale in the Bowland Basin, where both type II and type III kerogen are observed. Palci *et al.* (2020) increased and decreased the primary and secondary cracking activation energy of the kinetic reaction of Yang *et al.* (2015) by 3 kcal mol^{-1} to model the high and low-case scenarios for the Gainsborough Trough, respectively. Palci *et al.*'s (2020) sensitivity analyses show that the kinetic reaction plays a critical role in the generated and expelled hydrocarbons and hydrocarbon component distribution. Palci *et al.*'s (2020) adaptation of the kinetic reaction of Yang *et al.* (2015) is applied to the 2D modelling within the Bowland Basin.

Thermal boundary conditions

The results from 1D basin modelling at Thistleton-1 and Hesketh-1 are applied to constrain palaeo heat flow and estimates of erosion. A value for maximum heat flow during Early Cretaceous rifting of 65 ± 5 mW m^{-2} is assumed (Allen and Allen 2013). Late Cretaceous palaeo heat flows were 62.5 and 70 mW m^{-2} at Thistleton-1 and Hesketh-1, respectively. The results of AFTA analysis indicate that peak palaeotemperatures of 90–100°C were reached in the Sherwood Sandstone at 80–70 Ma. For the purposes of 2D basin modelling, these results are interpreted to indicate the onset of erosion of at the Base Maastrictian (72.1 Ma). Values for Late Cretaceous–recent erosion of 1200 and 1500 m are applied at Thistleton-1 and Hesketh-1, respectively. Values for palaeo heat flow and Late Cretaceous–recent erosion fit within the ranges indicated by 1D modelling at individual wells. Biostratigraphic data (Fig. 2) were used to calculate PWDs and SWITs were calculated using Wygrala's (1989) method for a latitude of 53°.

Shale gas resource estimate

The total volumes of in-place hydrocarbons in the Lower Bowland Shale are 0.15, 0.29 and 0.42 TCF/mile for the low, medium and high case

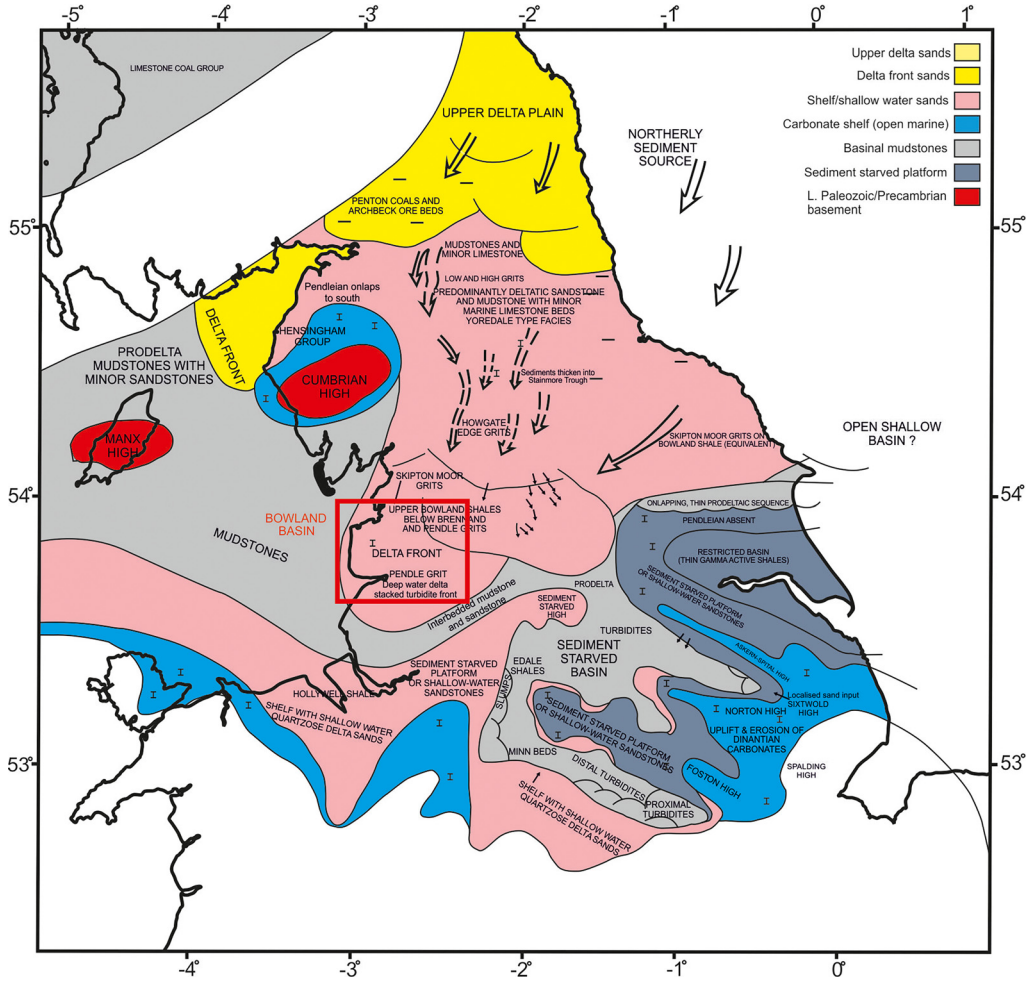

Fig. 7. Regional Brigantian–Early Pendlein palaeogeography across northern England. Note the different clastic sources for each sedimentary basin. The Bowland Basin is inclosed in the red box. Source: adapted from Fraser and Gawthorpe (2003).

scenarios, respectively. The total volumes of in-place hydrocarbons in the Upper Bowland Shale are 0.17, 0.33 and 0.48 TCF/mile for the low-, medium- and high case scenarios, respectively. The total volumes of in-place hydrocarbons accumulated in both the Upper and Lower Bowland Shale are 0.32, 0.62 and 0.90 TCF/mile for low-, medium- and high-case scenarios, respectively. Hydrocarbon accumulations in reservoirs are overwhelmingly dominated by hydrocarbon gases, with *c.* 35% methane, *c.* 13% ethane, *c.* 51% other gases (propane to *n*-pentane) and *c.* 1% hydrocarbon liquids. Hence, in-place hydrocarbon estimates correspond to GIP estimates. The 2D basin modelling results are summarized in Figure 8.

Using an approximate basin area of 3583 square miles, or 9281 km^2 (see Fig. 1 in Clarke *et al.* 2018), extrapolation of our 2D basin modelling results gives bulk shale GIP estimates of 68.5, 132.6 and 192.5 TCF for low-, medium- and high-case scenarios, respectively. Applying an approximate recovery factor of *c.* 10% thus yields total GIPs of 6.9, 13.3 and 19.3 TCF within the Upper and Lower Bowland Basin. Hence, these values yield a total shale gas resource estimate of *c.* 13.1 $\pm$ 6.4 TCF.

Hydrocarbon generation and conventional resource estimate

The total volumes of hydrocarbons generated (bulk generation balance) in the Lower Bowland

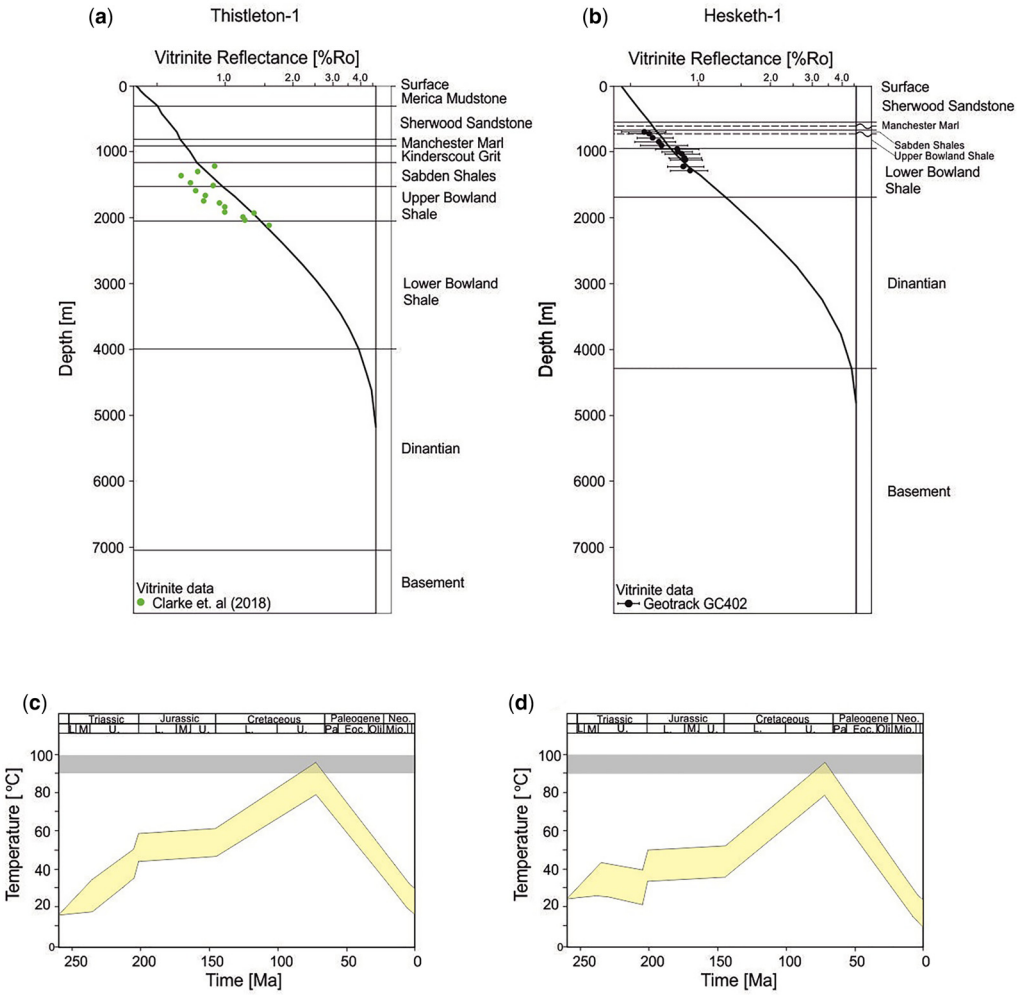

Fig. 8. 2D basin modelling results. (**a**, **b**) Thermal maturity profiles at wells Thistleton-1 and Hesketh-1, respectively (see Fig. 1 for well locations); (**c**, **d**) palaeotemperature profiles for Sherwood Sandstone at wells Thistleton-1 and Hesketh-1, respectively. Shaded regions, 90–100°C interval. Generated maturity and palaeotemperature profiles satisfy modelling conditions imposed from AFTA analyses and 1D basin modelling results.

Shale are 3.56, 6.09 and 8.37 TCF for the low-, medium- and high-case scenarios, respectively. The total volumes of hydrocarbons generated (bulk generation balance) in the Upper Bowland Shale are 1.19, 2.09 and 2.92 TCF for the low-, medium- and high-case scenarios, respectively. The total volumes of hydrocarbons accumulated in reservoirs are 0.22, 0.26 and 0.30 TCF for low-, medium- and high-case scenarios, respectively. Hydrocarbon accumulations in reservoirs are overwhelmingly dominated by hydrocarbon gases, with *c.* 35% methane, *c.* 13% ethane, *c.* 51% other gases (propane to *n*-pentane) and *c.* 1% hydrocarbon liquids. The 2D basin modelling results are summarized in Figure 8.

Discussion

Generation, maximum burial and loss of resources during uplift

Our results indicate that hydrocarbon generation within the Lower Bowland Shale begins during the Brigantian, north of the Summerer Fault and where shales reach depths of 3–4 km. Modest generation

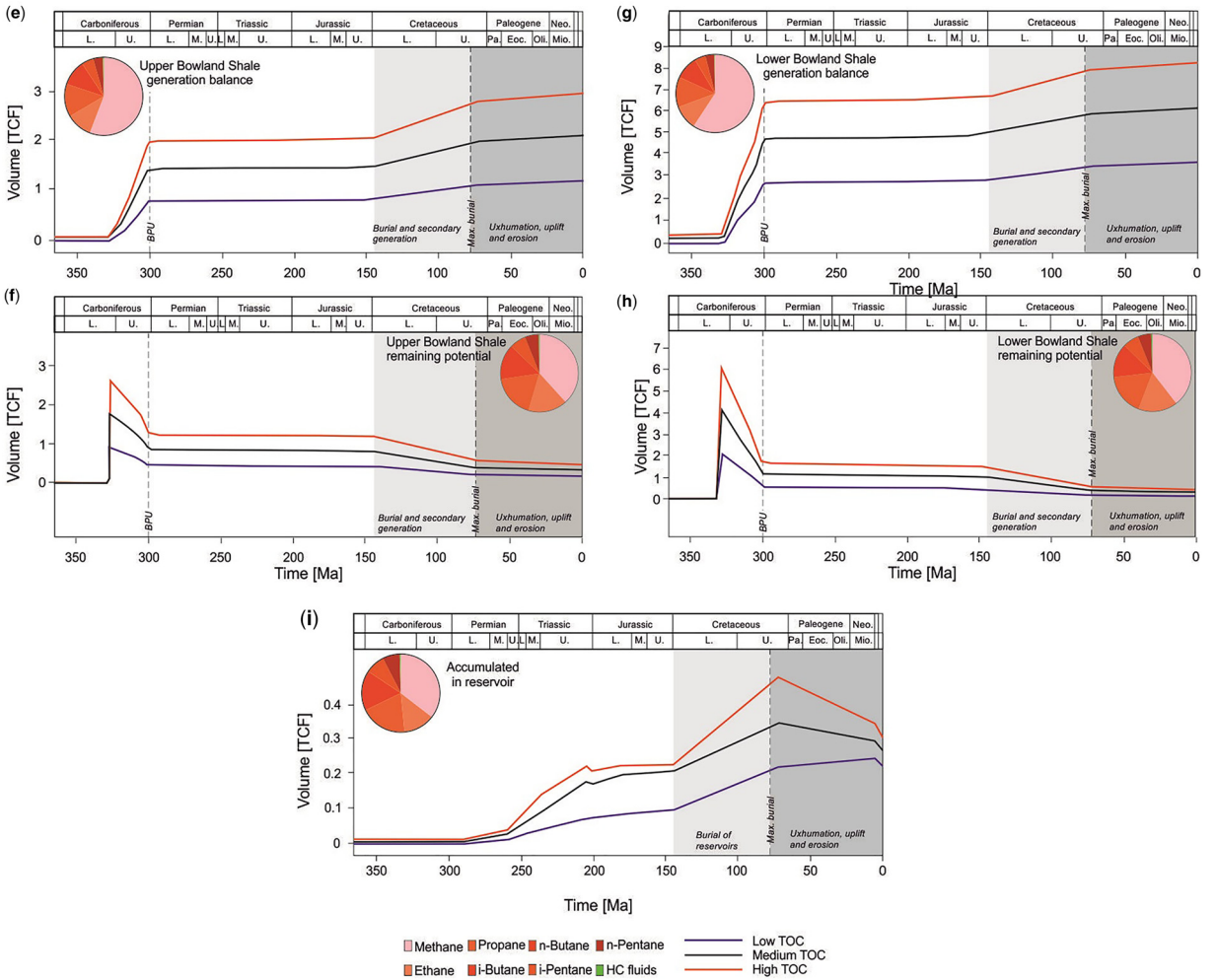

Fig. 8. *Continued*. (**e**–**h**) Hydrocarbon generation balance and remaining potential for Upper (**e** and **f**) and Lower (**g** and **h**) Bowland Shale, respectively. (**i**) Hydrocarbon accumulations in reservoirs; pie charts, hydrocarbon components; and shaded regions, timings of burial and exhumation.

within the Lower Bowland Shale during late Arnsbergian times is also seen south of the Pendle Fault within a syncline that reaches depths of 2.5–3 km. Hydrocarbon generation within the Upper Bowland Shale north of the Summerer fault and south of the Pendle fault begins during the Westphalian where depths reaches 3–4 km. Generation in both units continues throughout the Carboniferous, with increasing generation to the south of the basin. The TR of the Lower Bowland Shale reached *c.* 1 across the majority of the study area by the Late Carboniferous below 2500 m depth, indicating that the majority of kerogen had transformed into hydrocarbons by this time. However, above 2500 m the TR of the Upper Bowland Shale is <0.6 around the Thistleton Fault, Woodsford Fault and Hesketh Flower Structure (Fig. 9). Prior to the onset of Late Carboniferous–Permian erosion driven by the Variscan orogeny, the bases of the Upper and Lower Bowland shale reach maximum depths of 6.2 and 5.3 km north of the Summerer Fault.

A further period of secondary generation within the Upper Bowland Shale is indicated up to the point of maximum burial during the Late Cretaceous, whereby TR values reach *c.* 0.9–1 within the Bowland graben and south of the Pendle Fault. During this period, the bases of the Upper and Lower Bowland Shale reach maximum depths of 5.8 km and 6.8 km, respectively. Modest generation within the Lower Bowland Shale during this period is seen in a small region around the Bowland graben. The reason for the relatively high degree of hydrocarbon generation within the Upper Bowland Shale during this period is probably its shorter period of time within the generation window prior to Variscan erosion. Unlike the Upper Bowland Shale, the conditions required to place the Lower Bowland Shale within the oil and gas window existed for *c.* 25 Ma from Mid- to Late Carboniferous times. During this period, the Lower Bowland Shale is likely to have generated and expelled most of its hydrocarbons whilst the Upper Bowland Shale remained relatively under mature. The point of maximum burial is followed by the onset of exhumation, uplift and erosion of Cretaceous–Triassic strata across the basin. The AFTA analyses and 1D basin modelling results in this study allow for consideration of the impact of burial during the Cretaceous on hydrocarbon generation, and provides a geological hypothesis for the loss of in-place hydrocarbons in the Bowland Shale.

Our results indicate a resource potential significantly lower than that of previous works, e.g. Andrews (2013), and are remarkably close to recent

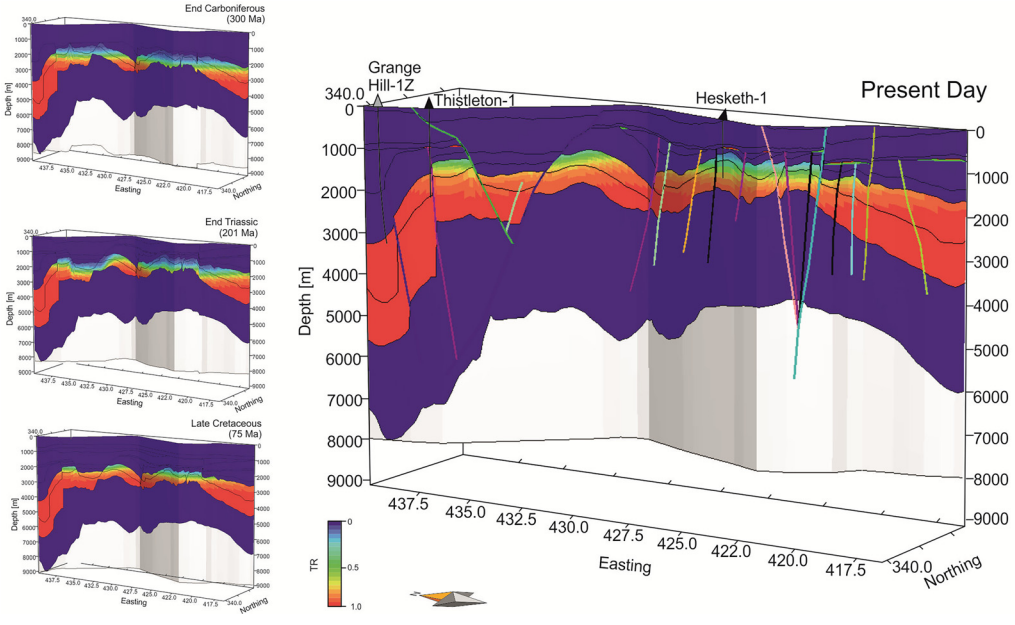

Fig. 9. Calculated transformation ratios within the Upper and Lower Bowland Shale at End Carboniferous, End Triassic, Late Cretaceous and present times. Non-source rocks have TR = 0. Present-day faults are shown by coloured lines. Triangles show the positions of wells, where black indicates intersected wells and grey projected. Location of modelled section shown in Figure 1.

estimates obtained by high-pressure water pyrolysis experiments (Whitelaw *et al.* 2019). Whilst the extrapolation of 2D basin modelling results applied in this study represents a significant simplification, this is the only work that considers the effect of post-Triassic burial and post-Cretaceous exhumation, uplift and erosion on resource potential across the basin. The importance of missing stratigraphy is often overlooked in many basin models, and in the case of the Bowland Basin has been completely ignored by previous work, e.g. Andrews (2013) and Whitelaw *et al.* (2019). Such events have the potential to significantly reduce the resource potential of many prospective unconventional and conventional hydrocarbon plays and must be considered during analysis. Our results also indicate that the volume of in-place conventional resources within reservoir intervals (Sherwood Sandstone and Kinderscout grit) was also significantly affected by post-Cretaceous exhumation. The GIP estimates within reservoirs decrease by *c.* 30–50% as a result of post-Cretaceous uplift, exhumation and erosion (Fig. 8). This decrease is most notable within the Sherwood Sandstone, where accumulations decreased by 60–70%.

The geological complexity of the Bowland Basin cannot be understated. The area evaluated in this study contains 18 modelled faults, but in reality contains a much greater and unknown number of near-vertical faults below seismic resolution. Reactivation of unknown faults is the primary cause of repeated events of induced seismicity that ultimately led the UK government to declare an indefinite moratorium on hydraulic fracturing and the abandonment of operations in the Bowland Basin. Whilst the Bowland Shale possesses all of the geochemical qualities required for a high-quality hydrocarbon source rock, a combination of geological complexity, basin compartmentalization and highly variable uplift, exhumation, erosion and palaeo heat flow across a relatively short distance (*c.* 100 km) renders the potential for economically recoverable reserves extremely low. However, these factors and the extensive coverage of the Bowland Shale across northern England raise the interesting possibilities of potential future work exploring carbon storage and geothermal resources.

Low-carbon resources

Given the recent moratorium on hydraulic fracturing in the UK, the emerging shale gas industry has been put on hold. A growing body of research indicates that shales preferentially adsorb up to 7 times more CO_2 than CH_4 at similar temperatures and pressures (e.g. Ansari *et al.* 2018). Adsorption of CO_2 to the surface of the host rock and desorption of the in-place CH_4 has several potential advantages over conventional carbon storage methods in shales, namely that adsorbed CO_2 remains fixed and does not dissolve into mobile fluids. This gives rise to the possibility that CO_2 injection into shales could displace CH_4, providing a means to reduce anthropogenic carbon and produce a commercial resource capable of being used as domestic fuel or as a source of hydrogen (e.g. Busch *et al.* 2008; Liu *et al.* 2019). However, the technique of enhanced CO_2 shale gas recovery is still in an early stage and must be investigated as a potential means to produce low-carbon resources in northern England. Despite the shale gas resource estimate from this and other recent studies being significantly lower than previous estimates, the possibility of simultaneously storing CO_2 while producing natural gas resource from the naturally fractured Bowland Shale presents an intriguing opportunity to reduce the UK's anthropogenic emissions while producing economic resources.

Geothermal resources

Present-day heat flow measurements from the Bowland Basin are between 50 and 60 mW m^{-2} in its centre and >70 mW m^{-2} in its NW region (Downing and Gray 1986). Hydrogeological data from depth in the region are sparse. In the nearby Cheshire Basin, porosities of 20% are considered likely and intrinsic transmissivity is believed to exceed 9.9×10^{12} m^3. Temperature data are widely scattered on a temperature–depth plot, but suggest a geothermal gradient of 27°C km^{-1}. Maximum temperatures at the base Permian are predicted to be almost 100° and at the base Sherwood Sandstone in excess of 80°C. A corrected bottom hole temperature of 81° C was measured at a depth of 3601 m in the Prees borehole within the basal Permian breccias. These high temperatures only occur over a few square kilometres, but temperatures in excess of 50°C are found over large areas, creating a large geothermal resource (Busby 2014). Furthermore, the fact that the Sherwood Sandstone reaches a maximum thickness of *c.* 1500 m and has widespread coverage across northern England and the Midlands raises the possibility of potential geothermal reservoirs that warrant further investigation (British Geological Survey 1999).

Conclusions

AFTAs indicate that peak palaeotemperatures of 90–100°C occurred within the Sherwood Sandstone during Late Cretaceous times at Hesketh-1. Application of this constraint to wells across the basin and 1D basin modelling indicates Late Cretaceous heat flow values of 62.5–80 mW m^{-2} and the erosion of

800–1500 m of post-Triassic strata. The cause of elevated Late Cretaceous heat flow remains unresolved; however, it is probably related to igneous intrusive activity within the larger East Irish Sea Basin, which the Bowland Basin forms part of.

We apply analysis of biostratigraphic data, apatite fission-track data and 1D basin modelling of wells within the Bowland Basin to constrain a regional 2D basin model and estimate hydrocarbon resource potential. Our results indicate that the Bowland Shale reached maximum burial during the Late Cretaceous and the basin was subsequently exhumed and <1500 m of post-Triassic strata were removed. Hydrocarbon generation in the Upper and Lower Bowland shale commenced during Westphalian and Brigantian times, respectively. A secondary phase of hydrocarbon generation primarily within the Upper Bowland Shale occurred during Cretaceous times up to the time of maximum burial. Post-Cretaceous uplift, exhumation and erosion across the basin reduced gas in place by <50%. Our results indicate that the shale gas resource potential of the Bowland Basin is *c.* 13.1 ± 6.4 TCF and is significantly lower than previous estimates obtained by regional mapping across northern and central England. Finally, we conclude that the geological and structural complexity of the Bowland Basin renders the region unsuitable for economic resources.

Acknowledgements Special thanks are given to Kelly Gallagher (University of Rennes) for access to QTQt thermochronological modelling software and Paul Green (Geotrack Intl.) for providing apatite fission-track data and expertise. Thanks are also due to Malcolm Butler (Beneath Britain) for providing access to regional seismic data. Recognition is given to the British Geological Survey for providing access to resources and workspaces that were essential for this work. Thanks are also due to Kieran Blacker for assistance with processing seismic data and discussions.

Competing interests The authors declare that they have no known competing financial interests or personal relationships that could have appeared to influence the work reported in this paper.

Author contributions **BHL**: conceptualization (lead), data curation (lead), formal analysis (lead), funding acquisition (lead), investigation (lead), methodology (lead), project administration (lead), resources (lead), software (lead), supervision (lead), validation (lead), visualization (lead), writing – original draft (lead), writing – review & editing (lead); **AP**: conceptualization (supporting), formal analysis (supporting), investigation (supporting), software (supporting); **AJF**: conceptualization (supporting), formal analysis (supporting), funding acquisition (supporting), investigation (supporting), methodology (supporting), project administration (supporting), resources (supporting), writing – original draft (supporting), writing – review & editing (supporting); **MN**: formal analysis (supporting), software (supporting); **JH**: conceptualization (supporting), data curation (supporting).

Funding The authors acknowledge support from the Natural Environment Research Council through the Unconventional Hydrocarbons in the UK Energy System Challenge 2 research programme (NE/R017964/1).

Data availability All data generated or analysed during this study are included in this published article.

Appendix

AFTA data

Tables A1–A4 contain AFTA data from samples GC402-17 and GC402-18 used in this study (from Green and Bray 1992). Both samples were collected from the Sherwood Sandstone at well Hesketh-1, at depths of 145 and 521 m for GC402-17 and GC402-18, respectively.

Table A1. *AFTA data for GC402-17 from Hesketh-1*

GC402-17				
Grain ID	N_s	N_i	Composition (wt% Cl)	Fission track age (Ma)
1	44	73	0.26	156.25 ± 30.0
2	9	17	0.045	137.44 ± 56.7
3	1	2	0	129.88 ± 159.1
4	12	42	0.007	74.54 ± 24.5
5	98	96	0.761	262.46 ± 38.1
7	43	72	0.041	154.84 ± 30.0
8	27	44	0.54	159.04 ± 39.0
9	7	14	0	129.89 ± 60.2
10	25	54	0	120.36 ± 29.2
11	19	29	0.034	169.67 ± 50.2
12	16	57	0.008	73.24 ± 20.8
13	21	53	0.091	103.14 ± 26.7
14	23	53	0.022	112.88 ± 28.2
15	14	56	0.022	65.27 ± 19.6
17	25	67	0.045	97.18 ± 22.9
18	48	166	0	75.43 ± 12.5
19	37	51	0.561	187.62 ± 40.7
20	4	13	0.016	80.24 ± 45.9
22	29	34	0.362	220.02 ± 55.8

Sample location: $X = 343\,001$, $Y = 425\,197$ (British National Grid coordinates), $Z = 145$ m and the stratigraphic unit is the Sherwood Sandstone (Triassic). Modelling parameters: $\zeta = 360.3$, $\rho_D = 1.46 \times 10^6$, $N_d = 2283$. Central age = 127.84 ± 13.1 Ma, pooled age = 132.28 Ma. Dispersion = 34.12%, $P(\chi^2) = 0$. Mean track length = 12.93, $\sigma = 2.216$.

Table A2. *AFTA data for GC402-18 from Hesketh-1*

GC402-18				
Grain ID	N_s	N_i	Composition	Fission track age (Ma)
1	2	3	0	171.97 ± 157.016
3	63	108	0.091	150.72 ± 24.058
4	20	117	0.004	44.53 ± 10.807
6	80	154	0.103	134.39 ± 18.69
8	55	206	0.212	69.42 ± 10.616
9	51	182	0	72.84 ± 11.62
10	26	75	0.134	90.00 ± 20.55
12	16	54	0.115	77.00 ± 21.963
13	27	48	0.055	145.40 ± 35.082
14	52	169	0.076	79.94 ± 12.764
15	15	50	0	77.95 ± 22.995
16	27	88	0	79.71 ± 17.6
17	15	45	0	86.56 ± 25.857
18	59	114	0.016	133.90 ± 21.618
19	14	36	0.039	100.87 ± 31.827
20	12	12	1.373	256.26 ± 104.727
21	12	52	0	60.05 ± 19.263
23	26	89	0.056	75.92 ± 16.984
24	9	14	0	165.90 ± 70.949

Sample location: $X = 343\,001$, $Y = 425\,197$ (British National Grid coordinates), $Z = 521$ m and the stratigraphic unit is the Sherwood Sandstone (Triassic). Modelling parameters: $\zeta = 360.3$, $\rho_D = 1.45 \times 10^6$, $N_d = 2283$. Central age = 95.51 ± 8.5 Ma, pooled age = 109.32 Ma. Dispersion = 28.18%, $P(\chi^2) = 0$. Mean track length = 12.67, $\sigma = 2.921$.

Table A3. *AFTA data from GC402-17 from Hesketh-1*

Grain ID	Track length (μm)	*C*-axis angle (°)
1	12.1	83.12
4	13.89	83.32
5	10.5	60.37
5	12.64	67
5	8.95	66.06
5	9.99	89.65
5	15.6	26.93
5	9.64	68.04
5	10.85	82.45
5	9.24	68.32
5	13.99	75.9
5	11.46	82.62
6	13.52	86
6	14.16	39.16
6	12.42	68.77
6	12.55	33.45
7	8.35	2.67
7	15.42	2.4
7	11.97	88.9
7	7.86	64.51
7	12.37	25.16
8	8.51	80.37
9	15.03	57.77
9	8.49	25.56
10	13.85	80.16
10	12.19	75.98
10	11.76	77.45
10	15.49	27.84
10	16.71	7.95
10	12.28	80.87
12	11.61	25.36
12	13.38	32.89
12	12.54	89.74
12	10.18	5.15
13	13.54	60.62
14	13.21	2.69
15	13.34	82.1
15	13.71	38.1
15	14.52	67.85
16	16.26	57.86
19	14.57	79.19
19	14.76	34.68
19	14.63	54.64
19	16.79	50.37
19	13.56	82.71
20	14.98	58.5
20	13.93	59.69
22	18.44	50.33
23	13.86	54.04
24	14.04	88.94
25	12.9	74.15
25	10.5	81.51
25	12.65	88.5
25	12.08	78.54
25	7.56	83.45
25	13.22	86.41
25	12.99	86.08
25	12.62	72.02
26	14.6	50.67
26	13.35	42.02
27	9.57	46.29
27	11.22	1.73
27	12.79	1.69
28	15.27	66.42
28	13.83	34.24
28	14.45	78.69
28	15.1	67.13
29	12.51	89.93
29	12.45	40.76
30	14.33	52.64
30	8.86	34.79
30	9.23	54.32
30	13.92	55.69
30	9.32	51.87
30	16.98	75.69
30	13.41	65.23
30	14.33	48.7
30	13.26	63.67
30	13.56	22.59
30	14.13	53.32

(*Continued*)

(*Continued*)

Table A3. *Continued.*

Grain ID	Track length (μm)	*C*-axis angle (°)
32	14.56	88.82
32	13.66	66.71
32	14.31	78.41
34	12.86	20.36
34	15.18	13.03
34	15.85	2.37
34	10.06	31.86
34	15.51	12.94
34	8.25	83.33
35	14.45	37.6
35	13.15	33.17
35	14.7	87.22
35	13.73	72.39
35	13.16	80.73
35	13.28	56.48
35	12.9	48.85
35	14.71	54.41
35	13.02	58.6
36	11.84	41.46
36	15.39	13.42
36	13.83	53.98
36	10.16	66.98

Table A4. *AFTA data from Sample GC402-18 from well Hesketh-1*

Grain ID	Track length (μm)	*C*-axis angle (°)
12	15.32	51.46
14	13.44	88.24
14	11.62	56.09
14	15.7	65.83
16	12.77	33.27
16	14.23	61.97
16	14.76	28.28
16	12.76	70.89
16	8.78	36.87
18	11.74	37.7
21	13.66	35.39
22	15.62	21.57
22	15.98	39.42
23	15.27	34.12
24	14.52	25.81
24	14.1	89.06
24	4.3	59.08
25	13.47	47.81
26	13.91	41.79
26	15.26	42.61
26	12.88	67.39
26	14.24	52.44
26	13.78	89.14
26	9.02	61.04
29	14.86	37.11
29	9.76	21.34
29	15.21	21.31
29	13.14	60.6
30	13.24	31.01
30	14.41	66.02
31	14.54	77.81
31	13.1	53.52
31	14.65	14.91
32	13.99	56.78
32	8.52	24.62
32	9.46	30.19
32	15.55	71.3
34	14.57	5.91
34	9.81	6.01
35	15.6	6.62
35	14.01	85.54
36	13.28	45.36
37	14.23	69.79
37	13.34	24.9
38	5.7	80.41
39	12.66	38.09
40	11.06	25.58
40	15.79	64.62
40	13.16	34.91
40	14.47	49.36
41	15.94	60.08
42	13.06	64.82
42	16.36	53.87
42	13.2	60.65
42	16.41	71.44
42	8.65	68.02
43	13.64	76.39
43	13.15	47.51
43	14.19	68.91
43	13.17	54.27
43	11.79	47.54
43	8.63	56.66
43	14.23	31.97
43	14.13	69.05
43	12.87	63.25
43	14.49	45.89
43	10.76	81.87
43	14.63	66.42
43	15.88	64.16
44	13.47	66.16
44	8.71	67.91
44	15.6	20.71
44	14.55	23.25
44	12.95	45.17
44	13.55	56.04
45	15.14	74.73
45	9.91	64.94
45	12.77	41.29
45	8.9	43.77
45	12.92	13.4
45	8.49	68.8
46	9.17	70.04
46	7.14	66.88
46	4.27	63.41
46	3.56	83.54
46	13.81	78.9
46	7	67.25

(*Continued*)

References

Allen, P.A. and Allen, J.R. 2013. *Basin Analysis: Principles and Application to Petroleum Play Assessment*. John Wiley & Sons.

Anderson, I. and Underhill, J.R. 2020. Structural constraints on Lower Carboniferous shale gas exploration in the Craven Basin, NW England. *Petroleum Geoscience*, **26**, 303–324, https://doi.org/10.1144/petgeo2019-125

Andrews, I. 2013. *The Carboniferous Bowland Shale Gas Study: Geology and Resource Estimation*. British Geological Survey Department of Energy and Climate Change, https://www.gov.uk/government/publications/bowland-shale-gas-study

Ansari, H., Joss, L., Trusler, M., Maitland, G., Delle Piane, C. and Pini, R. 2018. Enhanced shale gas recovery: gas sorption controls on recoverable gas and CO_2 storage capacity. *14th International Conference on Greenhouse Gas Control Technologies, GHGT-14*, 1–9, https://doi.org/10.2139/ssrn.3365806

Arthurton, R.S. 1983. The Skipton rock fault – an Hercynian wrench fault associated with the Skipton Anticline, northwest England. *Geological Journal*, **18**, 105–114, https://doi.org/10.1002/gj.3350180202

Arthurton, R.S. 1984. The Ribblesdale fold belt, NW England – a Dinantian–early Namurian dextral shear zone. *Geological Society, London, Special Publications*, **14**, 131–138, https://doi.org/10.1144/GSL.SP.1984.014.01.13

Bray, R.J., Green, P.F. and Duddy, I.R. 1992. Thermal history reconstruction using apatite fission track analysis and vitrinite reflectance: a case study from the UK East Midlands and Southern North Sea. *Geological Society, London, Special Publications*, **67**, 3–25, https://doi.org/10.1144/GSL.SP.1992.067.01.01

British Geological Survey 1999. *1:50,000 Scale Geological Map Sheet (England and Wales series)* **37**.

Busby, J. 2014. Geothermal energy in sedimentary basins in the UK. *Hydrogeology Journal*, **22**, 129–141, https://doi.org/10.1007/s10040-013-1054-4

Busch, A., Alles, S. *et al*. 2008. Carbon dioxide storage potential of shales. *International Journal of Greenhouse Gas Control*, **2**, 297–308, https://doi.org/10.1016/j.ijggc.2008.03.003

Charsley, T.J. 1984. *Early Carboniferous Rocks of the Swinden No. 1 Borehole, West of Skipton*. British Geological Survey Report **1611**, 5–12.

Clarke, H., Turner, P., Bustin, R.M., Riley, N. and Besly, B. 2018. Shale gas resources of the Bowland Basin, NW England: a holistic study. *Petroleum Geoscience*, **24**, 287–322, https://doi.org/10.1144/petgeo2017-066

Collinson, J. 1988. Controls on Namurian sedimentation in the Central Province basins of northern England. *In*: Besly, B.M. and Kelling, G. (eds) *Sedimentation in a Synorogenic Basin Complex: The Upper Carboniferous of Northwest Europe*. Chapman & Hall, Glasgow, UK, 85–101.

Corfield, S.M., Gawthorpe, R.L., Gage, M., Fraser, A.J. and Besly, B.M. 1996. Inversion tectonics of the Variscan foreland of the British Isles. *Journal of the Geological Society, London*, **153**, 17–32, https://doi.org/10.1144/gsjgs.153.1.0017

Daly, A. and Edman, J. 1987. Loss of organic carbon from source rocks during thermal maturation. *AAPG Bulletin*, **71**, 546.

Dewey, J. 1982. Plate tectonics and the evolution of the British Isles. *Journal of the Geological Society, London*, **1**, 371–412, https://doi.org/10.1144/gsjgs.139.4.0371

Donnelly, L.J. 2006. A review of coal mining induced fault reactivation in Great Britain. *Quarterly Journal of Engineering Geology and Hydrogeology*, **39**, 5–50, https://doi.org/10.1144/1470-9236/05-015

Downing, R.A. and Gray, D.A. 1986. Geothermal resources of the United Kingdom. *Journal of the Geological Society, London*, **143**, 499–507, https://doi.org/10.1144/gsjgs.143.3.0499

Earp, J., Poole, E. and Whiteman, A. 1961. *Geology of the Country Around Clitheroe and Nelson*, **68**. HM Stationery Office.

Falcon, N. and Kent, P. 1960. Geological results of petroleum exploration in Britain 1945–1957. *Geological Society, London, Memoirs*, **2**, 5–56.

Fraser, A.J. and Gawthorpe, R.L. 1990. Tectono-stratigraphic development and hydrocarbon habitat of the Carboniferous in northern England. *Geological Society, London, Special Publications*, **55**, 49–86, https://doi.org/10.1144/GSL.SP.1990.055.01.03

Fraser, A. and Gawthorpe, R.L. 2003. Palaeogeography and facies evolution, in: an atlas of Carboniferous Basin evolution in Northern England. *Geological Society, London, Memoirs*, **28**, 27–49, https://doi.org/10.1144/GSL.MEM.2003.028.01.04

Gallagher, K. 2012. Transdimensional inverse thermal history modeling for quantitative thermochronology. *Journal of Geophysical Research*, **117**, 1–16, https://doi.org/10.1029/2011JB008825

Gawthorpe, R.L. 1986. Sedimentation during carbonate ramp-to-slope evolution in a tectonically active area: Bowland Basin (Dinantian), Northern England. *Sedimentology* **33**, 185–206.

Gawthorpe, R.L. 1987. Tectono-sedimentary evolution of the Bowland Basin, N England, during the Dinantian. *Journal of the Geological Society, London*, **144**, 59–71, https://doi.org/10.1144/gsjgs.144.1.0059

Green, P. and Bray, R. 1992. *East Irish Sea Basin: Thermal and Tectonic Development and Hydrocarbon Generation Assessed Using Apatite Fission Track Analysis and Vitrinite Reflectance Phase 2*. Unpublished technical Report **GC402**.

Green, P., Duddy, I. and Bray, R. 1995. Applications of thermal history reconstruction in inverted basins. *Geological Society, London, Special Publications*, **88**, 149–165, https://doi.org/10.1144/GSL.SP.1995.088.01.10

Green, P.F., Duddy, I.R. and Bray, R.J. 1997. Variation in thermal history styles around the Irish Sea and adjacent areas: implications for hydrocarbon occurrence and tectonic evolution. *Geological Society, London, Special Publications*, **124**, 73–93, https://doi.org/10.1144/GSL.SP.1997.124.01.06

Green, P.F., Thomson, K. and Hudson, J.D. 2001. Recognition of tectonic events in undeformed regions: contrasting results from the Midland Platform and East Midlands Shelf, Central England. *Journal of the*

Geological Society, London, **158**, 59–73, https://doi.org/10.1144/jgs.158.1.59

Green, P.F., Duddy, I.R. and Hegarty, K.A. 2002. Quantifying exhumation from apatite fission-track analysis and vitrinite reflectance data: precision, accuracy and latest results from the Atlantic margin of NW Europe. *Geological Society, London, Special Publications*, **196**, 331–354, https://doi.org/10.1144/GSL.SP.2002.196.01.18

Gross, D., Sachsenhofer, R.F., Bechtel, A., Pytlak, L., Rupprecht, B. and Wegerer, E. 2015. Organic geochemistry of Mississippian shales (Bowland Shale Formation) in central Britain: implications for depositional environment, source rock and gas shale potential. *Marine and Petroleum Geology*, **59**, 1–21, https://doi.org/10.1016/j.marpetgeo.2014.07.022

Guion, P., Gutteridge, P. and Davies, S. 2000. Carboniferous sedimentation and volcanism on the Laurussian margin. *In*: Woodcock, N. and Strachan, R. (eds) *Geological History of Britain and Ireland*. Blackwell Science, Oxford, 227–271.

Hantschel, T. and Kauerauf, A. 2009. *Fundamentals of Basin and Petroleum Systems Modeling*. Springer.

Holford, S.P., Turner, J.P. and Green, P. 2005. Reconstructing the Mesozoic–Cenozoic exhumation history of the Irish Sea basin system using apatite fission track analysis and vitrinite reflectance data. *Geological Society, London, Petroleum Geology Conference Series*, **6**, 1095–1107, https://doi.org/10.1144/0061095

Holford, S.P., Turner, J.P., Green, P.F. and Hillis, R.R. 2009. Signature of cryptic sedimentary basin inversion revealed by shale compaction data in the Irish Sea, western British Isles. *Tectonics*, **28**, https://doi.org/10.1029/2008TC002359

Immenhauser, A. 2009. Estimating palaeo-water depth from the physical rock record. *Earth-Science Reviews*, **96**, 107–139, https://doi.org/10.1016/j.earscirev.2009.06.003

Jarvie, D. 2012. Shale resource systems for oil and gas: part 1 – shale-gas resource systems. *AAPG Memoirs*, **97**, 69–87, https://doi.org/10.1306/13321446M973489

Ketcham, R.A., Carter, A. and Hurford, A.J. 2015. Inter-laboratory comparison of fission track confined length and etch figure measurements in apatite. *American Mineralogist*, **100**, 1452–1468, https://doi.org/10.2138/am-2015-5167

Liu, D., Li, Y., Yang, S. and Agarwal, R.K. 2019. CO_2 sequestration with enhanced shale gas recovery. *Energy Sources, Part A: Recovery, Utilization, and Environmental Effects*, **43**, 3227–3237, https://doi.org/10.1080/15567036.2019.1587069

McDannell, K.T., Pinet, N. and Issler, D.R. 2022. Exhuming the Canadian Shield: preliminary interpretations from low-temperature thermochronology and significance for the sedimentary succession of the Hudson Bay Basin. *Geological Society of Canada Bulletin*, **609**, 287–322, https://doi.org/10.4095/326100

Nantanoi, S., Rodríguez-Pradilla, G. and Verdon, J. 2022. 3D seismic interpretation and fault slip potential analysis from hydraulic fracturing in the Bowland Shale, UK. *Petroleum Geoscience*, **28**, https://doi.org/10.1144/petgeo2021-057

Palci, F., Fraser, A.J., Neumaier, M., Goode, T., Parkin, K. and Wilson, T. 2020. Shale oil and gas resource evaluation through 3D basin and petroleum systems modelling: a case study from the East Midlands, onshore UK. *Petroleum Geoscience*, **26**, 525–543, https://doi.org/10.1144/petgeo2019-069

Peters, K.E., Walters, C.C. and Moldowan, J.M. 2005. *The Biomarker Guide*. Vols. **1** and **2**. 2nd edn. Cambridge University Press.

Pharaoh, T.C., Gent, C.M. *et al*. 2018. An overlooked play? Structure, stratigraphy and hydrocarbon prospectivity of the Carboniferous in the East Irish Sea–North Channel basin complex. *Geological Society, London, Special Publications*, **471**, 281–316, https://doi.org/10.1144/SP471.7

Timmerman, M.J. 2004. Timing, geodynamic setting and character of Permo-Carboniferous magmatism in the foreland of the Variscan Orogen, NW Europe. *Geological Society, London, Special Publications*, **223**, 41–74, https://doi.org/10.1144/GSL.SP.2004.223.01.03

Torsvik, T., Carlos, D., Mosar, J., Cocks, L. and Malme, T. 2002. Global reconstructions and North Atlantic paleogeography 440 Ma to recent. *In*: *BATLAS – Mid Norway Plate Reconstructions Atlas with Global and Atlantic Perspectives*. Geological Survey of Norway, Trondheim, 18–39.

US Energy Administration Information 2015. *Technically Recoverable Shale Oil and Shale Gas Resources: Jordan*. Technical Report, http://www.eia.gov/analysis/studies/worldshalegas/

Whitelaw, P., Uguna, C.N. *et al*. 2019. Shale gas reserve evaluation by laboratory pyrolysis and gas holding capacity consistent with field data. *Nature Communications*, **10**, 3659, https://doi.org/10.1038/s41467-019-11653-4

Wygrala, B. 1989. *Integrated Study of an Oil Field in the Southern Po Basin, Northern Italy*. PhD thesis, University of Cologne, Germany.

Yang, S., Horsfield, B., Mahlstedt, N., Stephenson, M. and Könitzer, S. 2015. On the primary and secondary petroleum generating characteristics of the Bowland Shale, northern England. *Journal of the Geological Society, London*, **173**, 292–305, https://doi.org/10.1144/jgs2015-056